Monthly Notices
of the
ROYAL ASTRONOMICAL SOCIETY

MNRAS **429,** 2001–2018 (2013) doi:10.1093/mnras/sts463

150 new transiting planet candidates from *Kepler* Q1–Q6 data

X. Huang,⋆ G. Á. Bakos and J. D. Hartman

Department of Astrophysical Sciences, 4 Ivy Lane, Peyton Hall, Princeton University, Princeton, NJ 08544, USA

Accepted 2012 November 21. Received 2012 November 19; in original form 2012 May 25

ABSTRACT

We have performed an extensive search for planet candidates in the publicly available *Kepler* long cadence data from quarters Q1 through Q6. The search method consists of initial detrending of the data, applying the trend filtering algorithm, searching for transit signals with the Box Least Squares fitting method in three frequency domains, visual inspection of the potential transit candidates and an in-depth analysis of the shortlisted candidates. In this paper we present 150 new periodic planet candidates and seven single transit events, 72 of which are in multiple systems. The periods of these planet candidates vary from ∼0.17 to ∼440 d. 124 of the planet candidates have radii smaller than 3 $R_{\oplus}$. We recover 82.5 per cent of the Batalha et al. Kepler Objects of Interest (KOI) catalogue. We also report 40 newly identified false positives – systems that look like transiting planets, but are probably due to blended eclipsing binaries. Our search improves the statistics in the short-period and small-planet radii parameter ranges.

Key words: planets and satellites: detection – planetary systems.

1 INTRODUCTION

The field of transiting extrasolar planets (TEPs) has exploded over the past few years. One major contributor is the *Kepler Space Mission*, continuously monitoring 156 000 stars in a 115 deg^2 field (Borucki et al. 2010; Koch et al. 2010). Since its launch in 2009, it has found 2321 planetary transit candidates[1] (Borucki et al. 2011a; Batalha et al. 2012, hereafter B12). The first four months of data (Q1 and Q2) yielded 1235 planet candidates associated with 997 host stars, including 60 confirmed planets around 33 stars (Borucki et al. 2011b, hereafter B11). The *Kepler* team has developed increasingly sophisticated procedures to identify planet candidates (Smith et al. 2012) and multiple systems (Ford et al. 2012; Steffen et al. 2012). Using more data (16 months) and improved detection procedures [the Transit Planet Search (TPS) algorithm; Jenkins et al. 2010c; Tenenbaum et al. 2012, hereafter T12], the total number of planet candidates has almost doubled since the release by B11 (B12).

An independent search with different tools can build confidence in the reliability of the detections, and the completeness of the sample, by e.g. providing new candidates that were missed by the *Kepler* science team. One such effort is the citizen science initiative, called PlanetHunters (Fischer et al. 2012; Lintott et al. 2012), based on the idea of Zooniverse (Lintott et al. 2008). Making use of human eyes to search for transit-like events through a user friendly computer interface, six new planet candidates were published by far (Fischer et al. 2012; Lintott et al. 2012). These were then subjected to the vetting procedure of the *Kepler* team, and five of them survived this process, i.e. they are not false alarms, as much as it can be determined from the *Kepler* data. However, conducting a visual search of all the raw light curves takes a lot of human effort. Quoted from Fischer et al. (2012): 'it is impractical for a single individual to review each of the ∼150 000 light curves in every quarterly release of the *Kepler* data base'. While challenging, it is, however, feasible for an individual to examine ∼150 000 light curves, if sophisticated computer algorithms narrow down the list to a somewhat smaller sample of candidate transits that can be then checked very carefully. Also, note that small planets are often hard to recover by visual inspection without phase-folding the light curve at the suspected periodicity of the signal.

Encouraged by these observations, we started an independent search for transiting planet candidates in *Kepler*'s long-cadence (LC) data. *Kepler* observations are grouped into so-called quarters (each having a duration of 3 months, except for Q0 and Q1, which are shorter). At the end of each quarter, the spacecraft rotates 90°, to adjust its solar panels. The majority of *Kepler* stars are observed as LC targets, for which data are obtained by gathering over 270 exposures within 29.4 min; 512 stars are also observed in short-cadence (SC) mode with 58.9 s intervals (Gilliland et al. 2010; Jenkins et al. 2010b; Murphy 2012). We used quarters Q0–Q6 in this search, which data were released to the public in 2012 January.

Our methodology is based on our experience conducting a similar search with HATNet (Bakos et al. 2004), a wide-field ground-based survey. Broadly speaking, the *Kepler* space-based data are of much higher quality than any ground-based data. Ground-based observations often exhibit large gaps in the time series, either due to the rotation of the Earth, or inclement weather conditions. The data quality

⋆ E-mail: xuhuang@princeton.edu

[1] http://kepler.nasa.gov/Mission/discoveries/candidates/

is highly variable due to changing extinction, clouds, background, seeing, etc. The per-point photometric precision is typically worse than from space, partly because of the above effects of ground-based observations, and partly due to the use of inexpensive hardware (e.g. front illuminated CCDs). Altogether, our ground-based data are of lower signal-to-noise ratio (SNR), has inhomogeneous quality and exhibits complex systematic variations with long gaps. For example, not a single transit event has been found in HATNet data by direct visual inspection; transits are detected through sophisticated data mining and phase-folding. Also, no robust *single* transit event was ever found by HATNet. Consequently, tools developed for a transit search using ground-based data may be very efficient in recovering transit signals from *Kepler*.

In this paper we employ tools from the transit detection pipeline of the HATNet project, after sufficient modifications to conform to the *Kepler* data. We also develop a pre-filtering method that corrects the *Kepler* light curves for known anomalies and systematics, before searching them for transit events. Our search is blind in the sense that the list of *Kepler* candidates was not consulted during the search.

The structure of the paper is constructed as follows. The data processing methodology is discussed in Section 2. We laid out our findings in Section 3, including the recovery of Kepler planet catalogue, our selection and modelling of new candidates, and the properties of these new candidates. We make our concluding remarks in Section 4.

2 DATA ANALYSIS

2.1 Removal of points and long trend filtering

We make use of the *Kepler* public LC light curves. We begin with the TIME and SAP_FLUX (raw flux) columns in the FITS (Flexible Image Transport System) files. The raw flux is already corrected for cosmic rays and background variations by the *Kepler* team (Jenkins et al. 2010a). First we convert the fluxes to magnitudes and set the mean value for each star to its *Kepler* magnitude taken from the Kepler Input catalogue (KIC).[2]

The second step is to clean the light curves based on the data anomalies table in the *Kepler Data Release Notes* for each quarter (Machalek et al. 2010, 2011; Christiansen et al. 2012a,b). We summarize all the important events in Q1 through Q6 in Table 1. We also describe the definition of anomaly types (adopted from *Kepler Data Characteristic Hand Book*) and our methods of correction for each type in the table notations. Generally, for data anomalies involving a discontinuity we model the jump by a polynomial with an offset in magnitude after the gap. The fitting uses 50 points on both sides around the gap. The offset is then subtracted from the data after the jump. In the time range during safe modes (Q2 and Q4), or Earth point recoveries (Q3, Q4 and Q6), there is an exponential decay in the flux. We identify and remove the whole exponential decay rather than attempting to correct for the effect.

Most of the stars exhibit long-term trends. We follow the traditional high-pass filter method (Ahmed, Natarajan & Rao 1974; Mazeh & Faigler 2010), and apply a cosine filter on all the cleaned light curves. For each light curve, before computing the filter, we generate a model by applying a 100 point (∼2 d long) median filter. This is done to prevent distortions due to outlier points (including introducing spurious 'transit' signals). The cosine filter is then computed as the sum of a linear component and $N = T_{\rm total}/\Delta T$ cosine functions, where the highest frequency is $1/\Delta T$ ($\Delta T = 1$ d), and $T_{\rm total}$ is the total time-span of the light curve:

$$M(t_j) = a\frac{(t_j - t_s)}{T_{\rm total}} + \sum_{i=0,N} b_i \cos\left[i\pi\frac{(t_j - t_s)}{T_{\rm total}}\right]. \quad (1)$$

Here t_j is the time of the jth measurement, and t_s is the first time instance in the light curve. The coefficient a for the linear component and coefficient b_i for the ith cosine functions are computed by a least-squares fitting procedure on the model. The fitted trend $M(t_j)$ is then subtracted from the light curves. We apply this cosine filter to light curves in every quarter separately, and then combine the long trend filtered light curves from Q1–Q6 by offsetting the magnitude of all the quarters referring to the magnitude of Q1.

[2] http://tdc-www.harvard.edu/software/catalogs/kic.html

Table 1. Anomaly summary table.

Start (BJD-245 4000)	End (BJD-245 4000)	Quarter	Anomaly type
1002.5198	1002.7241	2	EXCLUDE [a]
1014.5146	1016.7214	2	SAFE MODE [b]
1033.2932	1033.3341	2	TWEAK [c]
1056.4853	1056.8313	2	COARSE POINT [d]
1063.2896	1064.3726	2	EARTH POINT [e]
1073.3632	1073.3632	2	ARGABRIGHTENING [f]
1079.1866	1079.1866	2	TWEAK
1080.8008	1080.8212	2	ARGABRIGHTENING
1088.4018	1089.3213	2	COARSE POINT
1093.2239	1093.2239	3	EARTH POINT
1100.4163	1100.5389	3	COARSE POINT
1104.5233	1104.5438	3	COARSE POINT
1113.4116	1117.3346	3	MEMORY ERROR [g]
1123.5461	1124.4248	3	EARTH POINT
1206.2584	1206.2584	4	TWEAK
1216.4137	1217.3128	4	EARTH POINT
1229.8386	1233.8231	4	SAFE MODE
1307.9995	1309.2869	5	–
1336.7713	1337.6091	5	–
1399.5042	1400.3828	6	EARTH POINT
1431.2374	1432.1978	6	EARTH POINT

[a] EXCLUDE: manually excluded cadence before pipeline processing.
[b] SAFE MODE: due to unanticipated sensitivity to cosmic radiation, or unanticipated responses to command sequences. The amplitude of flux is affected after the end date of safe mode; data for additional 3 d are removed rather than corrected. Data on both sides are offset in magnitude to ensure continuity by a polynomial fit.
[c] TWEAK (Attitude Tweaks): discontinuities in the data due to small attitude adjustments. The discontinuities are corrected by offsetting the data on both sides using a polynomial fit.
[d] COARSE POINT (Loss of Fine Pointing): due to losing fine pointing control, removed.
[e] EARTH POINT: change of attitude due to monthly data downlink. Affect data the same way as safe mode. Corrected by the same method as safe mode.
[f] ARGABRIGHTENING: diffuse illumination of the focal plane. Removed. Only ARGABRIGHTENING events longer than one cadence are listed here.
[g] MEMORY ERROR: due to onboard spacecraft errors, gapped by the pipeline, the continuity on both ends of a gap is checked. Only a single memory error longer than one cadence is listed here.
[h] The format of data release handbook 8 for Q5 data is different from other quarters. There are no safe mode, tweak, coarse point or exclude phenomena in Q5, only two big gaps, possibly due to Earth point, are listed.

2.2 Sky groups and systematic trend filtering

Following the long-term trend filtering procedure described above (Section 2.1), we then apply the trend filtering algorithm (TFA) developed by Kovács, Bakos & Noyes (2005) on the combined (Q1–Q6) light curves. The idea of TFA is to select a set of template light curves, which we assume to contain information of the systematic variations, and then construct a linear filter based on their shared time series for each light curve to be corrected. TFA can remove systematic variations that are either shorter time-scale than those corrected by the cosine filter, or have an arbitrary functional form that is not well described by the sum of cosine functions. TFA assumes that the light curves are sampled at the same time-instances.

To construct a set of template light curves with the same time-base, we make use of the sky group information provided by the *Kepler* team. The sky group number is defined as the CCD channel number on which the stars fell during Q2 of the *Kepler* operation. *Kepler* has 21 modules. Each module contains two CCD chips and each CCD contains two output channels. The focal plain rotates 90° when the telescope switches to a new quarter every 3 months, except for the initial transition between quarters Q0 and Q1. Generally, the stars that belong to the same sky group share the same CCD channel all the time, although this channel changes from time to time. Therefore, each sky group shares the same time base, and has similar instrumental systematic trends. Additionally, stars in the same sky group are related in terms of their sky position, so that the local variabilities (e.g. local background variations or flux contamination from nearby stars) are often shared. TFA is designed to reduce this kind of general (shared by a number of stars) systematics.

We construct a separate filter for each sky group, selecting ∼300 template light curves in each case. Template stars are selected randomly, but in a manner that ensures a uniform distribution of their positions across the field. To exclude variable stars, we also impose a constraint on their median deviation around the median magnitudes (MAD, a quantity that is insensitive to outliers); stars with high MAD are ruled out from the templates. The total number of data points (time samples) in each template time base is ∼17 000–22 000, depending on the total length of time series in the sky group. In other words, we are not overfitting the light curves.

Altogether 124 840 stars in 84 sky groups were selected and analysed with TFA from the *Kepler* public LC data. For each sky group, we only selected stars that have been observed during the complete time range, and have not been affected by the failure of module 3. This is because the TFA analysis requires the same time-base to generate the filter per sky group. Module 3 failed in the middle of Q4, while observing sky groups 5, 6, 7 and 8. Due to the rotation of spacecraft, the Q5 data in sky groups 49, 50, 51 and 52, and the Q6 data in sky groups 77, 78, 79, and 80 were not available. Stars in these sky groups are still included if they have a complete data set in other quarters. Otherwise, we only selected light curves containing all the Q1–Q6 data (which has a total observation time of ∼500 d).

We note that the *Kepler* team has recently implemented a new 'cotrending' algorithm, called PDC-MAP (Smith et al. 2012). This algorithm uses 16 Cotrending Basis Vectors (CBV) that are generated by a singular value decomposition method applied separately to each channel and each quarter. This method has some commonalities with TFA. We did not make use of the PDC-MAP data, since they were not available for the Q1–Q6 data when we started our analysis.

In Fig. 1 we demonstrate our filtering process on a randomly selected light curve (KIC 003346154). The great improvement by the procedure is clearly demonstrated.

2.3 Box least-square fitting and transit analysis

We use the box least-square fitting (BLS) algorithm (Kovács, Zucker & Mazeh 2002) to search for periodic transit signals in the TFA-filtered light curves. In order to maximize the efficiency of the BLS search in a wide frequency range, we divide the frequency search into three, only slightly overlapping frequency domains: $0.3\,\mathrm{d}^{-1} < f_1 < 9.0\,\mathrm{d}^{-1}$, $0.02\,\mathrm{d}^{-1} < f_2 < 1.0\,\mathrm{d}^{-1}$ and $0.005\,\mathrm{d}^{-1} < f_3 < 0.03\,\mathrm{d}^{-1}$. We use a different number of frequency steps and BLS bins in each domain. We use the SNR (measured in the BLS spectrum) and DSP (dip significance) parameters (for details, see Kovács et al. 2002) of the first five frequency peaks reported by BLS to select candidate transit signals for manual inspection.

We adopt selection threshold of 11 and 8.5 for SNR and DSP in the middle- and long-period range. The selection threshold of short-period range is somewhat higher (30 and 20 for SNR and DSP) considering that BLS tends to respond to short period easier and there are fewer Kepler Objects of Interests (KOIs) in this period range as our reference. On top of these requirements, we neglect the BLS peaks with frequency too close to the frequency domain boundary (i.e. the period ranges used in selection are $0.67\,\mathrm{d}^{-1} < f_1' < 6.67\,\mathrm{d}^{-1}$, $0.0202\,\mathrm{d}^{-1} < f_2' < 0.67\,\mathrm{d}^{-1}$ and $0.005\,\mathrm{d}^{-1} < f_3' < 0.0202\,\mathrm{d}^{-1}$). We also reject those with a transit duration much longer than expected ($q_1 < 0.5$, $q_2 < 0.1$ and $q_3 < 0.013$) or a transit depth indicating very large planetary radius (dip > 0.04). These are not optimized selection criteria, but instead ensure that no shallow or rare transit events are missed. The low detection threshold also means that events will require close visual inspection. With the above limits, we selected ∼10 per cent of the stars to fold with the BLS peaks that satisfy the above requirements. The number of BLS peaks selected is ∼3 per cent of all the first five best BLS peaks. We then manually inspected all the folded light curves.

We take three random sky groups as an example to illustrate our selection process in Fig. 2. We show the distribution of BLS peaks (the mid period range) in the SNR-DSP plane. The solid lines are our lower limits for selection. The green dots are selected periods for further examination. The best BLS peak of KOI planet candidates is represented with red crosses. Majority of the KOIs are selected with high SNR and DSP.

Transit-like features in the folded light curves are flagged and further examined in the visual inspection. We reject light curves with recognizable depth variation for odd and even peaks. We also check the harmonics of the detected period to ensure the detection of a correct period. For the transits visible in the unfolded light curves, we directly inspect the shape and transit centre of each transit; for the transits invisible in the unfolded light curves (due to low signal-to-noise ratio), we perform phase-folding with the BLS-detected frequency before examining the data.

3 RESULTS

3.1 Comparison of our sample to that of the Kepler team

We flagged 2180 stars as possible transiting planet hosts during manual inspection. Among them, we found 180 stars which are

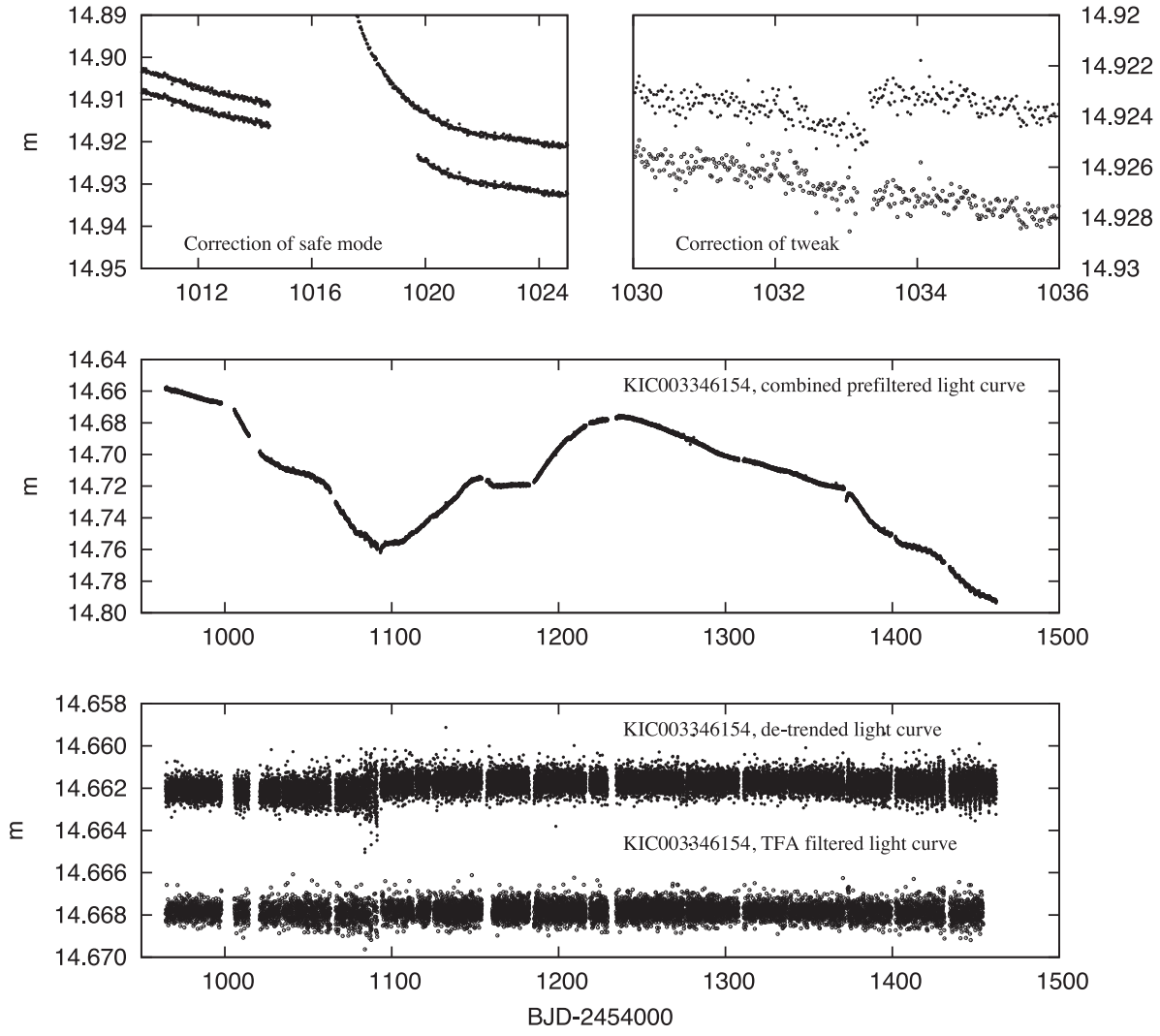

Figure 1. An example of our filtering process as applied to the light curve of KIC 003346154. The ordinate is in the units of approximate *Kepler* magnitude: Top panel: correction of safe mode (left) and tweak (right), (the example is taken from Q2). The corrected light curve is plotted below the uncorrected one. Middle panel: combined light curve from Q1 to Q6 after the pre-filtering process, i.e. correction of anomalous data points and combining the light curves from all the quarters. Bottom panel: light curve after long trend filtering (solid symbols) and after TFA (empty circles).

categorized as eclipsing binaries (EB)[3] (Prša et al. 2011) or false positives (FP)[4] (B11) by the *Kepler* team. We also cross-matched our results with the KOI catalogue[5] (Borucki et al. 2011a; B12; B11). We note that our detection efficiency is comparable to the TPS algorithm used by the Kepler team (T12). Their algorithm yields 5392 detections and detected 88.1 per cent of the 1235 KOIs in the B11 catalogue using data from Q1 to Q3. We recovered 92 per cent of the B11 catalogue in our analysis (1124 of the KOIs in B11 are in our initial data set from which 1034 are flagged) thanks to the longer time base we used compared to T12.

We demonstrate the selection of KOIs compared to the B12 catalogue in Fig. 3. There are 1518 KOI stars (corresponding to 1982 KOI planet candidates) from the B12 catalogue included in our overall LC light curve samples. The rest of the KOI stars in the B12 catalogue either fail to fulfil our LC time baseline length requirement (see Section 2.2) or have transit depths greater than 0.04, and are therefore rejected by our procedure. We found that 1311 (86.4 per cent) of the KOI stars are flagged in our selection process. 1636 (82.5 per cent) of the KOI planet candidates are detected (either with the correct period reported by BLS or are detected with the wrong period but later recovered during visual inspection).

We failed to recover about 17.5 per cent of the KOI planet candidates, mostly due to no significant peaks found in the BLS spectra corresponding to the transit periods. This partly results from the choice of BLS parameters and also the non-periodic properties of some transit signals. The hard cut in DSP is the second most important reason for the rejection of some KOI planetary candidates. Some KOIs have low DSP due to either overcorrection of our light curves or light curves with high noise level. There are also 40 KOI planet candidates with BLS peaks selected by our pipeline but rejected during visual inspection. From further investigation, we find that 32 of these rejected transit signals are not visible when folded with twice the detected periods, probably due to strong transit timing variations. A detailed detection report of all the KOIs is presented in Table 2. We do not model the KOIs unless the host stars are

[3] http://archive.stsci.edu/kepler/eclipsing_binaries.html
[4] http://archive.stsci.edu/kepler/false_positives.html
[5] http://archive.stsci.edu/kepler/planet_candidates.html

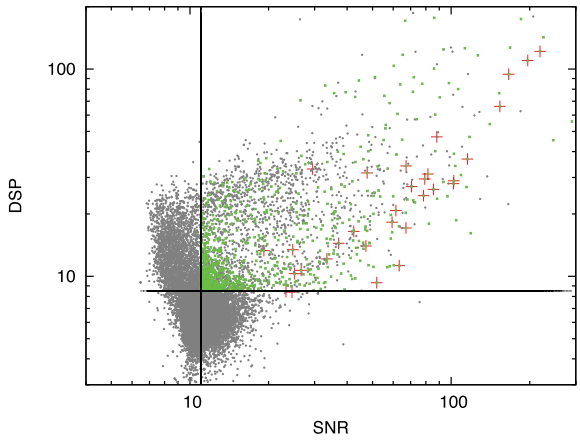

Figure 2. A demonstration of our selection methods. SNR versus DSP for all the first five BLS peaks from stars in sky groups 1, 12 and 19 (black dots). Solid lines present the lowest limit of SNR and DSP for selection. Green asteroids resemble all the BLS peaks actually selected for folding considering the period range and transit duration. Red crosses show the most significant peak of all the KOI planet candidates (34 in total) in these sky groups.

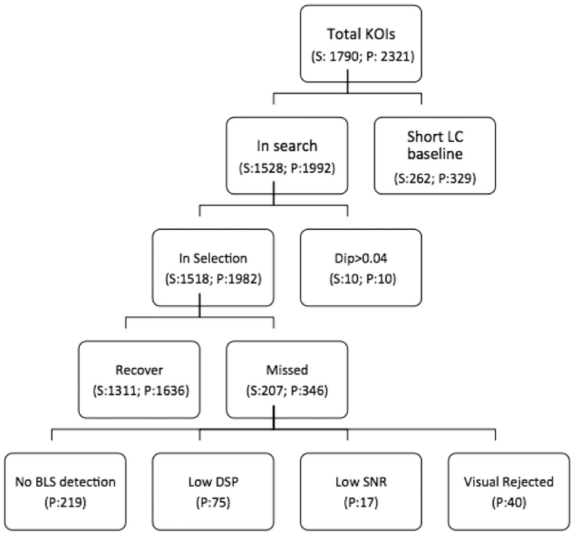

Figure 3. Summary of our recovery of KOIs in the B12 catalogue. We show the number of stars (S) and planet candidates (P) in each category. The recovery rate of KOI host stars in our search range is 86.4 per cent. The recovery rate of KOI planet candidates is 82.5 per cent. For more information, see Section 3.1 and Table 2.

found to have other high SNR and DSP transit signals that are not reported by the Kepler team. The additional signals are treated as new candidates in our short list.

3.2 Generation of the planet candidate short list

We examined in detail the remaining candidates which are not included in the publicly available lists of candidates, EBs or FPs. We re-applied the cosine filter to these light curves constructed with a greater number of cosine functions and a smaller frequency interval. We aimed to clean systematic variations from the light curves (whether intrinsic to the stars, or due to instrumental effects), leaving flat light curves with transits. The cosine functions are generated in a frequency range adjusted according to the visual determination of the frequency of the stellar variation. To preserve the transit signal, we applied a median filter with a window width at least twice that of the detected transit duration, before generating the cosine filter. BLS was applied again on the corrected light curves. The first 10 peaks in the BLS spectrum are examined and compared to the previous detection, ensuring the detection of the transit signal is robust. As shown in Section 3.3, all candidates were checked against FP scenarios.

3.3 False positive detection and robustness checking

We use the moment-derived centroids provided by the *Kepler* FITS files to further eliminate possible FPs. For long-period planet candidates, we visually examine the centroids at the transit time. For short-period planet candidates, we examine the phase-folded centroid curves (de-trended by the cosine filter). We present one of our 'failed' transit candidates as an example in Fig.4. The folded light curve would naively suggest that there is a transit signal due to a planet with $R_{\rm p}/R_{\star} = 0.0198 \pm 0.0017$ and period of $P = 2.00783 \pm 3.8 \times 10^{-5}$ d. However, the phased centroids show a shift of ~0.004 pixels in the y direction during transit events, which indicates this is likely to be an FP signal due to a blended EB. According to the 2MASS (Two Micron All Sky Survey) image stamp, there is no nearby source within an area of 20 × 20 arcsec^2, i.e. the binary is not resolved in the 2MASS images. We provide a list of 40 FPs flagged by this method in Table 3. These stars have not been reported by the *Kepler* team in their FP lists. They are also not reported as candidates by the *Kepler* team. The stellar information and estimated shifts in both directions are also given in our table. We also used the public target pixel files and PyKE package[6] developed by the *Kepler* team, to obtain pixel light curves for all of our candidates with transit depths greater than 1 mmag. It is difficult to perform the same analysis on shallower transits, because of the low SNR of the events in the light curves of individual pixels.

Here we take one of our new detections, KIC 005437945, as an example for our photometry analysis. We detected four non-periodic transit events altogether, which could be explained as due to two long-period planet candidates with different epochs, depths and durations. The transits in Q1 and Q6 are due to a $P \approx 440$ d planet candidate; and the transits in Q2 and Q5 are due to a $P \approx 220$ d planet candidate (i.e. they are in a 2:1 resonance). We present the analysis for the transit event in Q6 here. We show the pixel image of out-of-transit, in-transit and the difference imaging in Fig. 5. The images are computed by plotting the mean out-of-transit flux (±2 d around the transit events), the mean in-transit flux and the difference between the two. The difference imaging during transit is identical to the out-of-transit flux distribution. No obvious background source is indicated for this particular star.

We further use the pixel calibration technique enabled by PyKE to extract light curves from every single pixel in the aperture. Fig. 6 shows the light curves extracted separately from 6 pixels in the Q6 aperture (the aperture is shown in Fig. 5). We can see that while the magnitude in every single pixel changes during the transit, they all show visible evidence for the transit event with roughly the same depth. The averaged flux from all the pixels has a flat out-of-transit magnitude. In addition, the centroids do not present an anomalous shift during the transit events.

[6] http://keplergo.arc.nasa.gov/ContributedSoftwarePyKEP.shtml

Table 2. Detection report of KOIs.[h]

KOI	KIC	Kepperiod (d)	Period (d)	Kepepoch (BJD-2454000)	Epoch (BJD-2454000)	Dip (mag)	Q^i	SNR	DSP	COMMENTS
1.01	11446443	2.470 613	–	955.762 57	–	–	–	–	–	sod [a]
2.01	10666592	2.204 735	2.204 760	954.357 80	965.378 28	6.10e-03	7.55e-02	206.05	179.41	
3.01	10748390	4.887 800	4.887 970	957.812 54	967.5793 24	2.60e-03	2.39e-02	439.78	55.43	
157.04	6541920	46.687 100	22.689 217	–	981.433 477	6.00e-04	1.11e-02	58.68	37.10	wp [b]
157.05	6541920	118.363 800	113.449 430	–	1026.812 678	8.00e-04	2.10e-03	15.36	21.01	wp
375.01	12356617	600.000 000	–	1072.223 82	–	–	–	–	–	snd [c]
1099.01	2853093	161.526 600	–	1031.001 52	–	–	–	32.38	5.94	ld [d]
1448.01	9705459	2.486 600	2.486 616	967.109 29	964.620 09	4.25e-02	4.46e-02	167.96	135.49	lr [e]
1888.01	10063802	120.019 000	–	967.182 56	–	–	–	10.05	13.06	ls [f]
2066.01	3239671	147.972 400	–	1096.090 06	–	–	–	−1.00	−1.00	nd [g]
...	...	...	...	...	...	...	...	...	...	...

[a] sod (short of data): KOIs do not have sufficient length of LC data to fulfil the requirement of TFA. They are not selected for our reanalysis.
[b] wp (wrong period): KOIs recovered with a wrong period. For some planet candidates, the harmonics of the KOI period (or other periods due to the imperfect correction of the light curve) show higher SNR and DSP in the BLS analysis. The SNR and DSP values reported here correspond to the detected signal instead of the KOI period. In other cases, frequencies not related to the signal are detected, the true signal is recovered in visual inspection, we fill the SNR and DSP with '—'.
[c] snd (single transit, no detection): KOIs with a single transit, and all the reported BLS peaks, are under our selection limits.
[d] ld (low DSP): KOIs with lower DSP than our selection limits, therefore not recovered in our selection process.
[e] lr (large radius): KOIs with transit dip larger than 0.04, therefore not selected for analysis.
[f] ls (low SNR): KOIs with lower SNR than our selection limits, therefore not recovered in our selection process.
[g] nd (no detection): KOIs for which the first five BLS peaks are under our selection limits, and the correct period is not one of the first five BLS peaks.
[h] We compare the parameters of KOIs with the B12 catalogue. The period, epoch, dip and q are taken from our BLS analysis instead of modelling the candidates. A complete version of this table can be accessed from the online version.
[i] Q: a dimensionless parameter representing the transit duration. Defined as $T_{\rm dur}/P$.

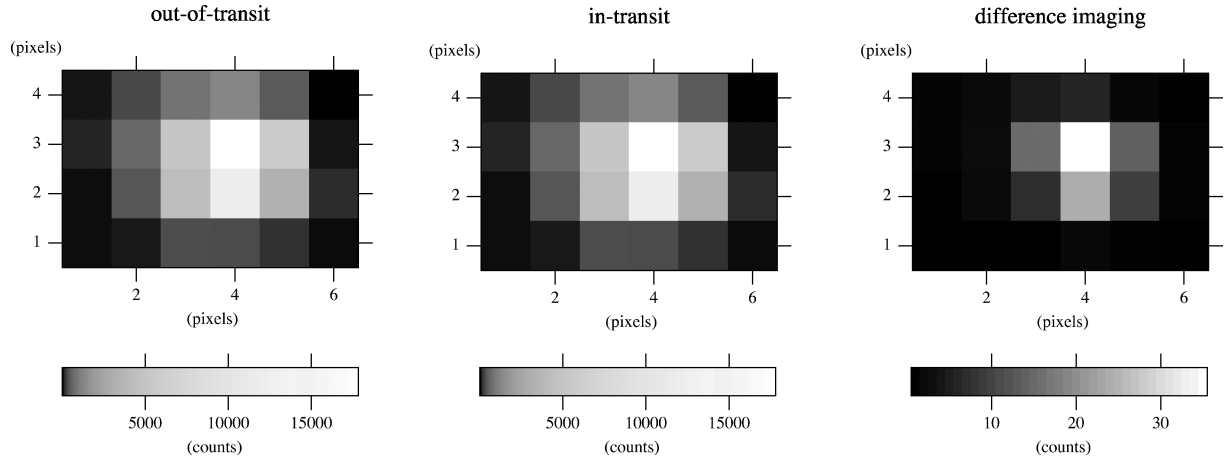

Figure 4. Light curves and centroids for KIC 004072333, phase-folded using the detected period and epoch. Top panel: phase-folded light curve (bottom) with period $P = 2.00783$ d and $E = 2455302.8774$ (BJD) and its residual from the fitting (top). Bottom panel: folded centroids in the x direction (top and grey) and the y direction (bottom and dark) with the same parameters. This detection is flagged as an FP due to the shift of centroids in the y direction during transit. There is no visible companion in the 2MASS image stamp within 20×20 arcsec^2 for this particular star.

For the rest of the transits which are not suitable for applying the single pixel analysis, we use other methods to at least ensure the robustness of the detection. We removed the detected transit signal according to the epoch, period and transit duration reported by BLS. Then we computed six different BLS spectra for each of the new light curves. The BLS spectra were obtained with three different sets of parameters (different frequency steps and bin numbers), each set of parameters is used twice. The first 10 peaks of every BLS spectrum were analysed. We compared these 60 frequency peaks to our original transit detections. For all of the planetary transit signals we analysed, the original periods as well as their harmonics were not detected in the transit-removed light curves.

Altogether 150 planet candidates entered our final list of new detections. The properties of their host stars are provided in Table 4. The detected periods range from ∼0.17 to ∼440 d. We also found six new multiple systems (altogether with 15 planet candidates) in stars not in the B12 catalogue. We found 57 new transit signals in KOI hosting stars; 43 of these are also independently reported by Ofir & Dreizler (2012, hereafter O12). We

Table 3. FP list.[a]

Star	Kepmag	RA (°)	Dec. (°)	Epoch (BJD-245 4000)	Period (d)	Displacement x^b (Pixel)	Displacement y^b (Pixel)	SNR
2442359	13.931	19 24 53.566	+37 46 53.58	965.8428	0.552 83	−0.0025	–	26.16
3336765	13.617	19 19 49.397	+38 27 49.07	965.1613	1.844 83	–	−0.000 32	38.93
3852258	13.819	19 27 55.433	+38 58 16.25	968.1106	5.758 38	–	0.005	17.48
4035667	10.035	18 58 29.566	+39 10 56.68	965.5837	2.873 66	−0.007	0.005	−1.00
4072333	15.664	19 41 19.236	+39 09 45.14	965.5638	2.007 75	–	0.0030	37.69
4077901	13.007	19 45 42.948	+39 08 01.54	967.7249	6.054 44	–	0.002	27.22
4270565	15.154	19 34 24.946	+39 23 18.96	972.2024	18.011 43	0.007	−0.007	28.47
5443775	12.936	19 21 20.671	+40 39 11.02	967.8765	3.307 54	–	−0.000 34	73.09
5565497[c]	11.521	19 57 31.702	+40 45 29.30	966.11575	1.412 532	−0.0126	−0.0011	131.4
5622812	12.832	19 30 41.270	+40 52 10.34	964.8384	0.103 04	−0.005	−0.005	49.76
5649325[c]	13.560	19 55 55.289	+40 52 19.34	1196.35	195.63	0.0016	–	7.81
...	...	...	...	...	...	...	...	...

[a]We only report the FPs not in the *Kepler* FP catalogue here. We do not report FPs in *single* transit events. These FPs are all identified by examining the centroids. We refer to the text for a detailed description of the method. A complete version of this table can be accessed from the online version.
[b] The flux centroid displacement amplitude is computed from the phase folded centroids. The x and y directions are listed separately. We do not list a displacement when the shift is not detected.
[c] There are visible companion(s) in the 2MASS image stamp within 20 × 20 arcsec^2.

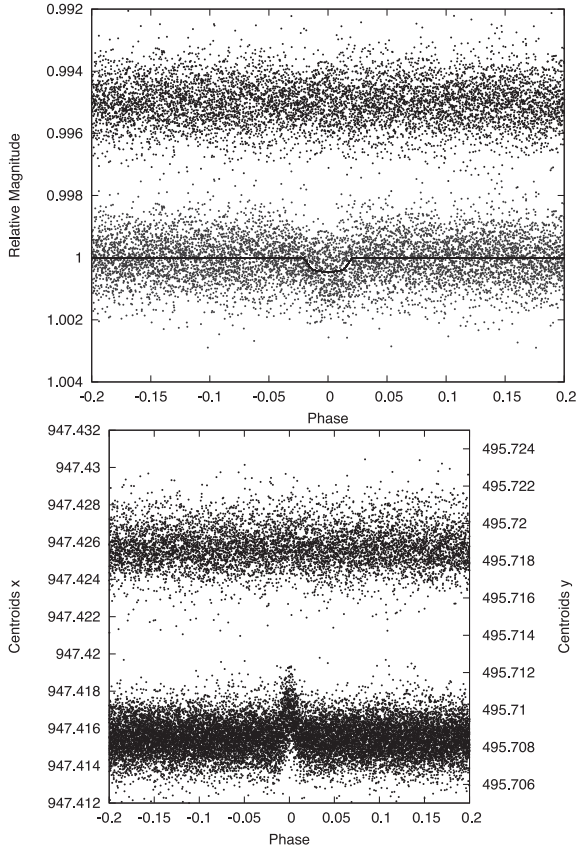

Figure 5. Out-of-transit image (in log scale of flux), in-transit image (in log scale of flux) and the difference between the two (in linear scale of flux) from the pixel files for KIC 005437945 Q6 transit. We do not see a visible shift in the flux distribution on the pixel image during transit, demonstrating that the apparent transit is not due to a variation of a background source.

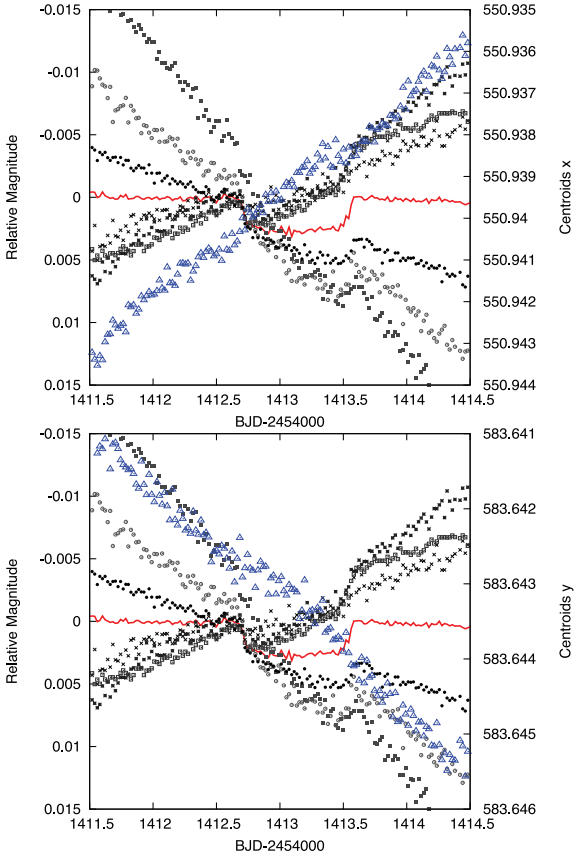

Figure 6. Red solid line: light curve flux for transit events in Q6 for KIC 005437945. Blue triangles: raw centroids x (top panel) and y (bottom panel). Different types of black points: light curves generated from different pixels separately in the aperture using KEPEXTRACT from the PyKE package.

also include seven *single* transit events. One of these single transit events is around a KOI star with a known planet candidate. Using the convention of B12 for single transit events, we assign a negative integer period number for these potential candidates. We compute the minimum allowed period according to the given time-span of the light curve and the epoch of transit. This is taken as the estimated period for single transit events in modelling.

Table 4. Stellar parameter table.[a]

Star	Kepmag	$T_{\rm eff}$ ($R_\odot$)	$\log g$ (K)	[Fe/H] (cgs)	$R_\star$	u_a [b]	u_b [c]
2985587	13.910	6023	4.278	−0.069	1.276	0.34	0.29
3128552	14.523	5530	4.673	−0.248	0.761	0.41	0.25
3240049	11.557	4435	2.127	−0.065	17.188	0.65	0.09
3245969	15.681	4825	4.789	0.054	0.594	0.59	0.13
3328026	15.147	5681	4.508	0.147	0.947	0.42	0.24
3345675	15.635	4105	4.628	0.137	0.598	0.57	0.17
3346154	14.575	5513	4.490	0.118	0.957	0.45	0.22
3439096	13.799	4940	3.119	−0.340	5.493	0.52	0.18
3541946	13.597	5537	4.728	−0.140	0.711	0.43	0.24
3558849	14.218	5938	4.432	−0.410	1.052	0.33	0.30
3728432	15.646	4371	4.583	−0.254	0.696	0.59	0.13
3764879	14.024	5845	4.641	0.006	0.809	0.38	0.27
3834322	15.397	4627	4.631	−0.004	0.698	0.62	0.11
4150804[d]	12.888	–	–	–	–	0.40	0.25
...	...	...	...	...	...	...	...

[a]A complete version of this table can be accessed from the online version of the paper.
[b]The quadratic limb darkening parameter a.
[c]The quadratic limb darkening parameter b.
[d]The limb darkening coefficient is obtained from the estimated stellar properties based on the *J*, *H* and *K* magnitudes.

3.4 Analysis

The transit modelling of all the candidates is based only on the *Kepler* light curves and the stellar parameters provided by the KIC. The parameters we can obtain directly from light curves are the transit depths, durations, ingress/egress durations and individual transit centres.

Without radial velocity (RV) data, mass determinations for these systems are generally not available. It may be possible to measure the masses through subtle photometric effects, like ellipsoidal variations and relativistic beaming (Mazeh & Faigler 2010; Kipping & Spiegel 2011). These effects are prominent for close binary stellar systems as well as massive planet companions (Loeb & Gaudi 2003). We did not observe these effects in our candidates.

The eccentricity is also unknown, although broad limits can be placed on the orbital configuration for very wide transits (Kipping 2008). An eccentric orbit could result in asymmetry in the transit light curves, as well as a shift in the mid-time of transits relative to the occultation events. In principle, the eccentricity could also be derived from modelling the detailed shape of a transit light curve. However, detecting these effects requires extremely high resolution and SNR light curves, which were not available for our candidates. Generally speaking, we observe no apparent asymmetry in any of our candidates, which suggests modest eccentricity or certain values of argument of periastron. We assume circular orbits in our modelling, following the convention of previous KOI modelling with only transit light curve information (B12).

We assume no flux dilution from blended nearby stars in our modelling. This is plausible for most of our candidates. We inspect the 2MASS image stamps with an area of 20×20 arcsec^2 centred on each target. Four of them have nearby companions, which are marked out in Table 5.

In theory, one could also fit for the limb darkening coefficients (LDC), but this requires very high SNR and well-sampled data, i.e. deep transits or many transit events (Kipping & Bakos 2011). We use a quadratic limb darkening formalism to model the transit light curves. The LDCs corresponding to the stellar atmospheres are interpolated with the stellar parameters from KIC in the ATLAS model grid LDCs provided by Sing (2010) for *Kepler*. The stellar parameters and the LDCs for the candidates are listed in Table 4. We also generate a grid of 1000 randomly selected stars from KIC with known stellar parameters and the interpolated their LDCs following the method described above. We then use these to determine LDCs for stars without information such as $T_{\rm eff}$, $\log g$ and [Fe/H] by linear interpolating in the *J*, *H*, *K* colour space. Since the LDCs obtained with this method have larger uncertainties, the derived planet parameters for planets without host star parameters provided by KIC should be treated with caution.

To conclude, in our transit modelling, we *do not* fit for:

(a) the planet mass $M_{\rm p}$;
(b) the eccentricity e of the orbit, which is assumed to be zero;
(c) the blending due to nearby stars, which is set to be zero;
(d) the LDCs of stars, which are computed as described above.

We did fit the following geometric parameters which correspond:

(a) the fractional planet radius $R_{\rm p}/R_\star$;
(b) the square of the impact parameter square b^2;
(c) the inverse of half duration $\zeta/R_\star = 2/T_{\rm dur}$.

This quantity is related to $a/R_\star$ for zero eccentricity via the relation:

$$\frac{\zeta}{R_*} = \frac{a}{R_*}\frac{2\pi}{P}\frac{1}{\sqrt{1-b^2}}. \quad (2)$$

In the fitting procedure we constrained the quantities b^2,$R_r/R_\star$,$\zeta/R_\star$ to be the same for each individual transit for a selected candidate.

We also fitted for the additional parameters of out-of-transit magnitudes and transit centres. For the short-period cases (with a period shorter than 30 d), we fit the median out-of-transit magnitude, first transit centre T_A and the last transit centre T_B as free parameters, with the total number of transits N fixed. We also assume that the transits are strictly periodic. We do not model the out-of-transit variation; the light curve is assumed to be flat. For our long-period candidates, we use a slightly different method. We take the out-of-transit magnitude and transit centres of individual transits as independent parameters, the total number of free parameters in the fit for a transit light curve with N transits is $2N + 3$. The periods of the candidates with only a single transit were estimated by the stellar density through KIC parameters, and by assuming no limb darkening and circular orbits (Yee & Gaudi 2008). The estimated periods for these cases are shorter than the lower limit constrained by the fact that only one transit event was observed during Q1–Q6. These single events were fitted as if they were an individual transit in a long-period system with a rough lower limit on the period.

In the fitting we used the formalism of Mandel & Agol (2002), and the methodology laid out in the analysis of HATNet planet discoveries (Bakos et al. 2010). A 10 000 step Markov Chain Monte Carlo (MCMC) simulation is then applied around the best-fitting parameters to explore the parameter space. The final reported planet parameters and estimated errors are taken as the median and median deviation of all the accepted jumps in the chain. The period is then recalculated by taking the median of $(T_B - T_A)/N$ for all the accepted jumps in the chain. We derive the transit number closest to the average of T_A and T_B (weighted by their errors as derived from the MCMC runs), and use the transit centre of this event (calculated from T_A, T_B, N) asthe optimal epoch.

Table 5. Planet candidates table.[a]

KIC	Epoch (BJD-245 4000)	σ_E (10^{-3})	Period (d)	σ_p (10^{-4})	R_p ($R_\oplus$)	$R_p/R_\star$	σ_R (10^{-3})	b	$\zeta/R_\star$ (d^{-1})	SNR	DSP	χ^2	Comments
2985587	1159.6256	1.5	3.375 816	0.52	1.640 40	0.011 78	0.84	0.68 ± 0.19	42.99 ± 2.9	40.83	14.78	1.44	
3128552	1219.6102	1.2	2.504 621	0.18	1.061 37	0.012 78	0.90	0.66 ± 0.19	24.26 ± 0.86	27.167	9.826	4.16	KOI2055 [b],O12 [c]
3128552	1298.5430	4.9	4.025 928	0.75	1.1627	0.0140	1.1	0.68 ± 0.18	16.91 ± 0.50	33.43	10.76	4.16	KOI2055,O12
3218908	1187.6632	1.2	4.152 573	0.54	0.9736	0.0128	0.96	0.64 ± 0.20	18.73 ± 0.61	27.1020	12.7280	4.09	KOI1108,O12
3240049	1234.98694	0.43	2.945 4270	0.094	61.9190	0.033 01	0.99	0.95 ± 0.037	23.61 ± 0.33	24.94	34.13	0.62	T12 [d]
3245969	1301.042	15	11.390 60	1.8	1.8410	0.0284	1.9	0.46 ± 0.38	20.4 ± 1.7	36.80	10.72	18.97	KOI1101,T12
3326377	1188.2283	1.8	198.7039	20	3.7018	0.0379	1.8	0.67 ± 0.15	6.127 ± 0.080	19.5130	24.9130	3.22	KOI1830,O12
3328026	1102.5054	1.7	2.115 515	0.39	1.75795	0.017 01	0.73	0.58 ± 0.12	10.6 ± 1.1	103.06	35.56	6.96	T12
3345675	1203.14403	0.12	120.002 673	0.80	14.73987	0.225 86	0.28	0.90 ± 0.00	26.70 ± 0.000	8.03	17.837	18.34	wp[e],PHt[f]
3346154	1231.72962	0.31	1.952 7041	0.057	1.855891	0.017 77	0.78	0.48 ± 0.20	53.7 ± 1.1	105.71	22.92	4.40	T12
3439096	1108.8290	1.3	2.975 892	0.21	7.61918	0.012 71	0.50	0.53 ± 0.17	11.74 ± 0.21	32.91	23.49	3.71	
3541946	1270.418	12	1.311 837	0.13	0.9854	0.0127	5.2	0.17 ± 0.83	20.6 ± 2.0	61.05	37.19	1.50	KOI624,O12
3558849	1112.9840	1.5	−258	–	6.677 80	0.058 17	0.61	0.34 ± 0.12	2.919 ± 0.013	-	-	2.11	
3728432	1314.79711	0.22	3.908 6360	0.043	1.920 17	0.025 28	0.47	0.30 ± 0.14	27.83 ± 0.20	107.92	19.85	15.22	T12
3764879	1118.75219	0.68	1.306 9750	0.067	1.3331	0.0151	1.0	0.73 ± 0.17	49.29 ± 1.80	112.23	31.15	1.69	T12
3834322	1087.18555	0.12	0.498 443 00	0.0040	0.991 03	0.013 01	0.47	0.46 ± 0.16	50.41 ± 0.68	17.46	7.65	8.90	T12
4150804	1271.38683	0.69	160.8818	10	–	0.079 85	0.64	0.365 ± 0.080	4.801 ± 0.013	12.06	24.85	0.35	PH[f]
4245933	1165.1932	1.9	11.256 29	1.3	0.812 85	0.014 08	0.45	0.46 ± 0.17	3.23 ± 0.027	25.29	11.88	13.00	T12
4271474	1262.46308	0.40	21.861 83	1.1	1.714 11	0.025 80	0.59	0.35 ± 0.14	15.71 ± 0.11	20.09	9.26	16.18	
4275117	1146.8945	5.1	2.0130 42	0.12	1.2924	0.0139	1.0	0.62 ± 0.18	43.66 ± 3.33	34.05	11.09	3.64	T12
4552729	1427.64700	0.16	97.461 490	0.62	4.174 580	0.039 153	1.1	0.47 ± 0.14	7.474 ± 0.078	44.69	10.07	3.68	PH
4858610	1128.2926	1.0	2.722 874	0.18	1.171 41	0.012 02	0.61	0.57 ± 0.18	16.72 ± 0.30	32.15	12.00	5.18	
4927315	1077.3419	1.5	11.768 56	1.5	1.9340	0.0192	1.2	0.67 ± 0.18	24.2 ± 1.1	31.24	17.07	3.49	T12
4951249	1072.5112	1.4	4.523 406	0.24	1.298 61	0.015 74	0.62	0.55 ± 0.18	18.02 ± 0.59	40.99	11.01	6.36	T12
5008501	1073.17351	0.38	0.968 0371	0.023	1.006 58	0.012 90	0.63	0.65 ± 0.18	55.4 ± 1.3	34.65	17.00	1.83	PH,T12
5023843	1320.7241	1.2	−358	–	6.1223	0.0543	1.5	0.3 ± 1.0	11.00 ± 0.15	–	–	2.83	PH
5128673	1353.1823	5.2	87.9654	36	2.250 57	0.027 46	0.44	0.1435 ± 0.0049	3.368 ± 0.048	28.37	8.66	2.81	blend[g]
...	...	...	...	...	...	...	...	...	...	...	...	...	...

[a] A complete version of this table can be accessed from the online version.
[b] Stars already identified as KOIs. The candidates presented here are transit signals that have not previously been detected in these systems.
[c] Planet candidates also identified by O12.
[d] Planet candidates classified as potential transit candidates by T12. If noted as T12t, the same signal is identified as a different set of parameters by T12.
[e] The signal is selected by a different period originally and then corrected by visual inspection. The SNR and DSP reported here correspond to the period we report here instead of the selected period.
[f] Planet candidates classified as potential transit candidates by PlanetHunters. If noted as PHt, the transit feature is identified by PlanetHunters but they did not report a period for comparison. These information can be accessed through http://www.planethunters.org.
[g] Systems may be blended by nearby stars. There exists a visible companion(s) within 20 arcsec^2 in a 2MASS image stamp centred on the target star.

3.5 Properties of candidates

We summarize the planet parameters for all the candidates in Table 5. The best-fitted model on the phase folded light curves and the residuals from the best-fitted model are presented in Figs 7–9 for long-period, short-period and single transit planet candidates.

We compare the planet candidates reported in this paper with the B12 catalogue KOIs in Fig. 10. Our new planet candidates follow a similar distribution in the SNR and DSP space as the KOIs. This demonstrates that our recovery of new candidates is due to the efficiency of our pipeline rather than due to a reduction in the selection thresholds. We also show in the right-hand panel of Fig. 10 that the majority of new candidates have short period (less than 10 d) and small transit depth. For comparison, we plot the KOIs missed by our search in green, suggesting that our detection sensitivity drops as the period of the transit signal increases.

We plot the period and planet radius (in units of host star radii) histogram in Fig. 11. The turn over points in both the period and radius space are modified with the supplementation of our new candidates. We suggest that our methods are more sensitive to short-period candidates since the detection efficiency of BLS is generally higher in high frequency. We also confirm that the KOI samples are almost complete in the mid-period range. We do not have much advantage in the long-period range over the original Kepler pipeline. The sample size around $P \sim 100$ d slightly gains with our new candidates. Signals with periods longer than 100 d usually suffer

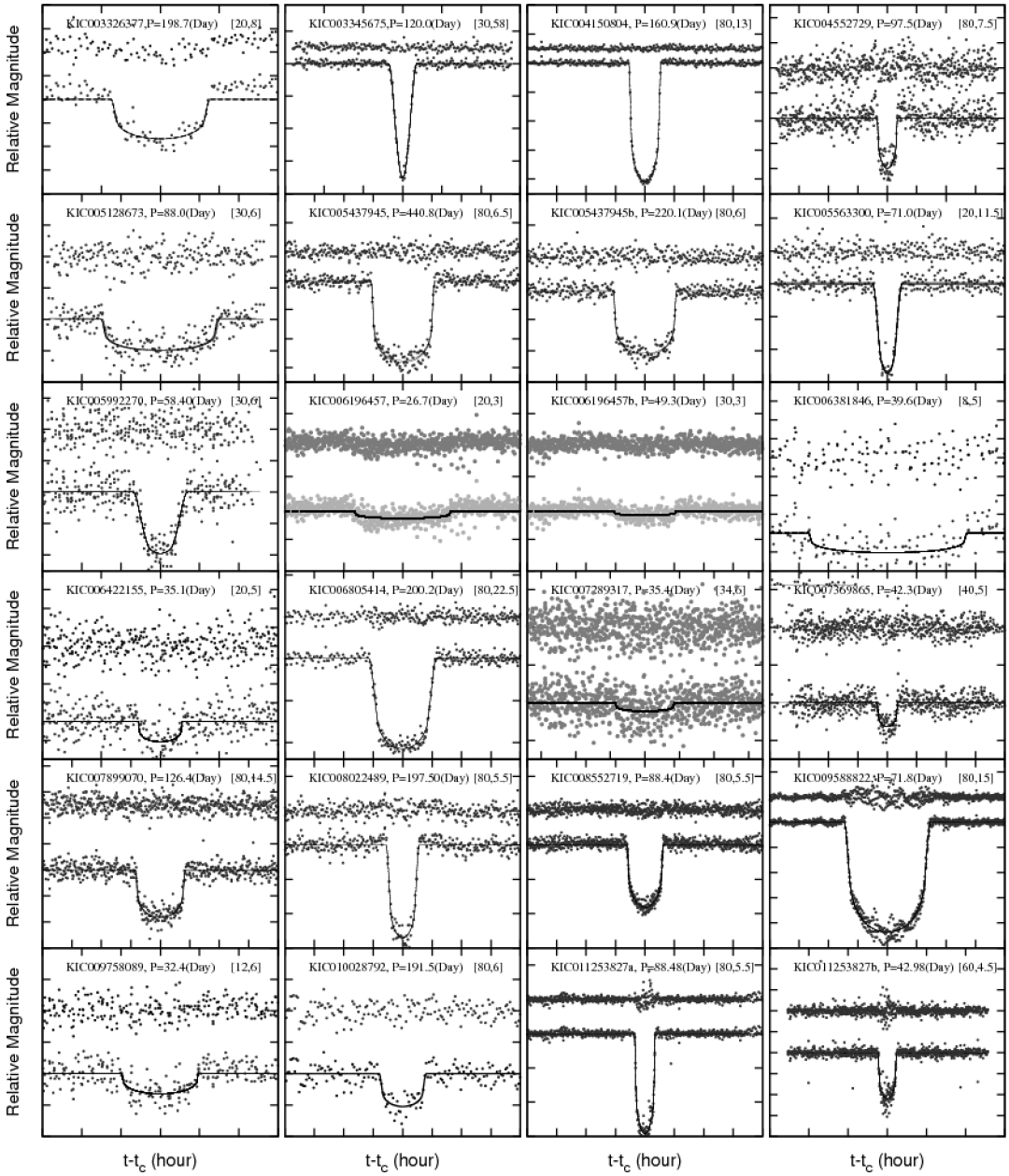

Figure 7. New long-period planet candidates. For each candidate we show the best-fitting model on the phase-folded light curve (bottom of the panel) and the residuals (top of the panel). For each candidate, we model all transits separately. We then fold the transits using the locally computed transit centres. We show the KIC number, period and scales of the figure of every planet candidate at the top of the subfigures. The *x*, *y* scales of the subfigure size are marked on the top right, in the units of (h, 1 mmag).

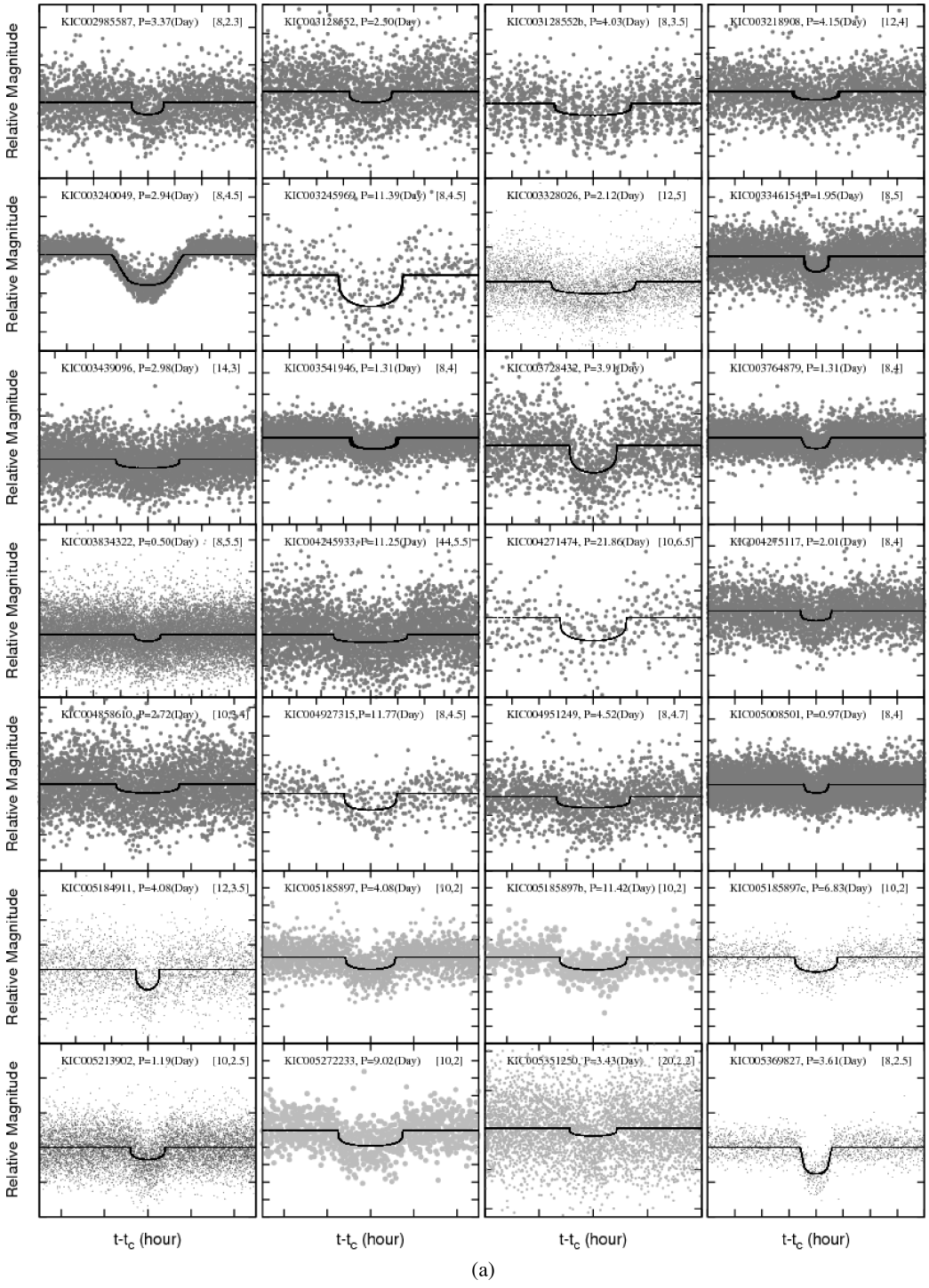

(a)

Figure 8. Short-period planet candidates. For each candidate we show the best-fitting model on the phase-folded light curve. The residuals are flat so we do not show them in the figures. The *x*, *y* scales of the subfigure size are marked on the top right, in the units of (h, 1 mmag).

from overcorrection of individual transit or low DSP simply because of lack of points in the transit phase.

Finally, we provide remarks on some of the interesting systems below.[7]

[7] The planet and stellar parameters we quote here are only approximated numbers for easy comparison. For accurate parameters and estimated errors, refer to Table 5.

KIC 005185897. We found three planet candidates in the system, all with transit depths ∼0.1 mmag. The periods of the candidates are 4.08 d (a), 11.42 d (b) and 6.83 d (c) (see Fig. 8a, row 6, Columns 2, 3 and 4). The stellar radius from KIC is only 0.51 $R_\odot$, which makes the modelled radii extremely small for all the candidates in the system. The $P = 11.42$ d signal and 4.08 d signal are modelled to be ∼0.62 $R_\oplus$, and the 6.83 d signal is slightly larger ($0.67R_\oplus$). They are also the smallest planet candidates we found around non-KOI stars. Both the pair b and c, c and a are around 5:3 resonance.

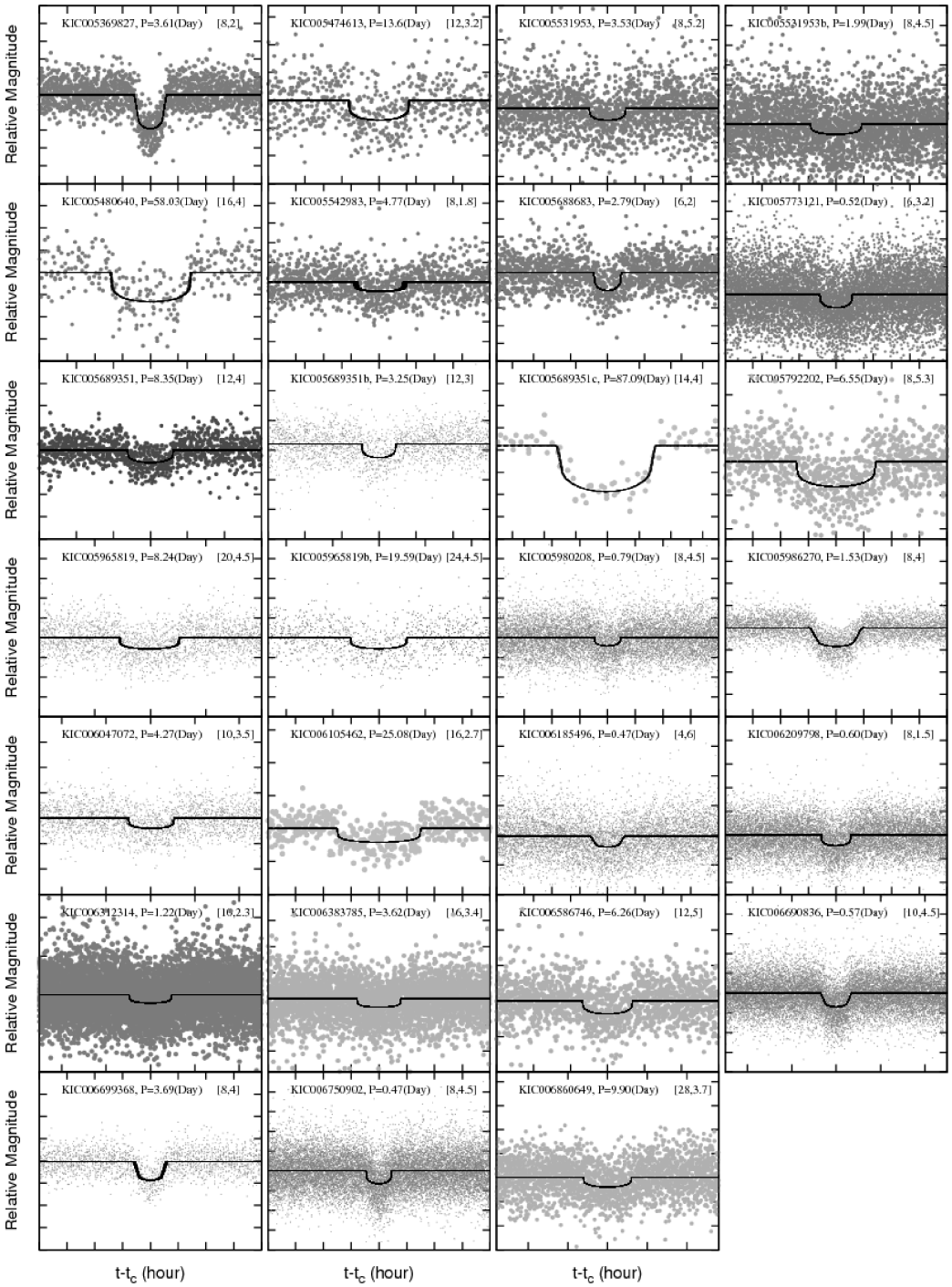

(b)

Figure 8 – *continued*

The planet candidate (a) was also found by the TPS algorithm as a potential transit signal (T12).

KIC 005437945. We identify four transit events in the light curve. The transit events in Q1 and Q6, and the ones in Q2 and Q5, share the same depths and durations, respectively. The former is modelled to be a 7.5 $R_\oplus$ planet candidate with 440 d period; the latter is modelled to be a 6.4 $R_\oplus$ planet candidate with a period of 220 d (see Fig. 7, row 2, Columns 2 and 3.) We note that the transit in Q1 is independently identified and classified as a single transit event by the Planet Hunters (Schwamb et al. 2012). A tweak happened during the transit in Q2 for the inner planet candidate; by carefully offsetting the magnitude on both sides of the tweak, we recover the full transit signal. We resolved a faint close companion (∼5 arcsec) in the Echelle slitviewer of the Apache Point Observatory 3.5-m telescope (see Fig. 12). We examined 2MASS image stamps in *J*,*H* and *K* and DSS 1,2 images in red and blue. All of the above show that the companion is bluer than KIC 005437945, which indicates that it is unlikely to be a physically associated companion. We present the phase

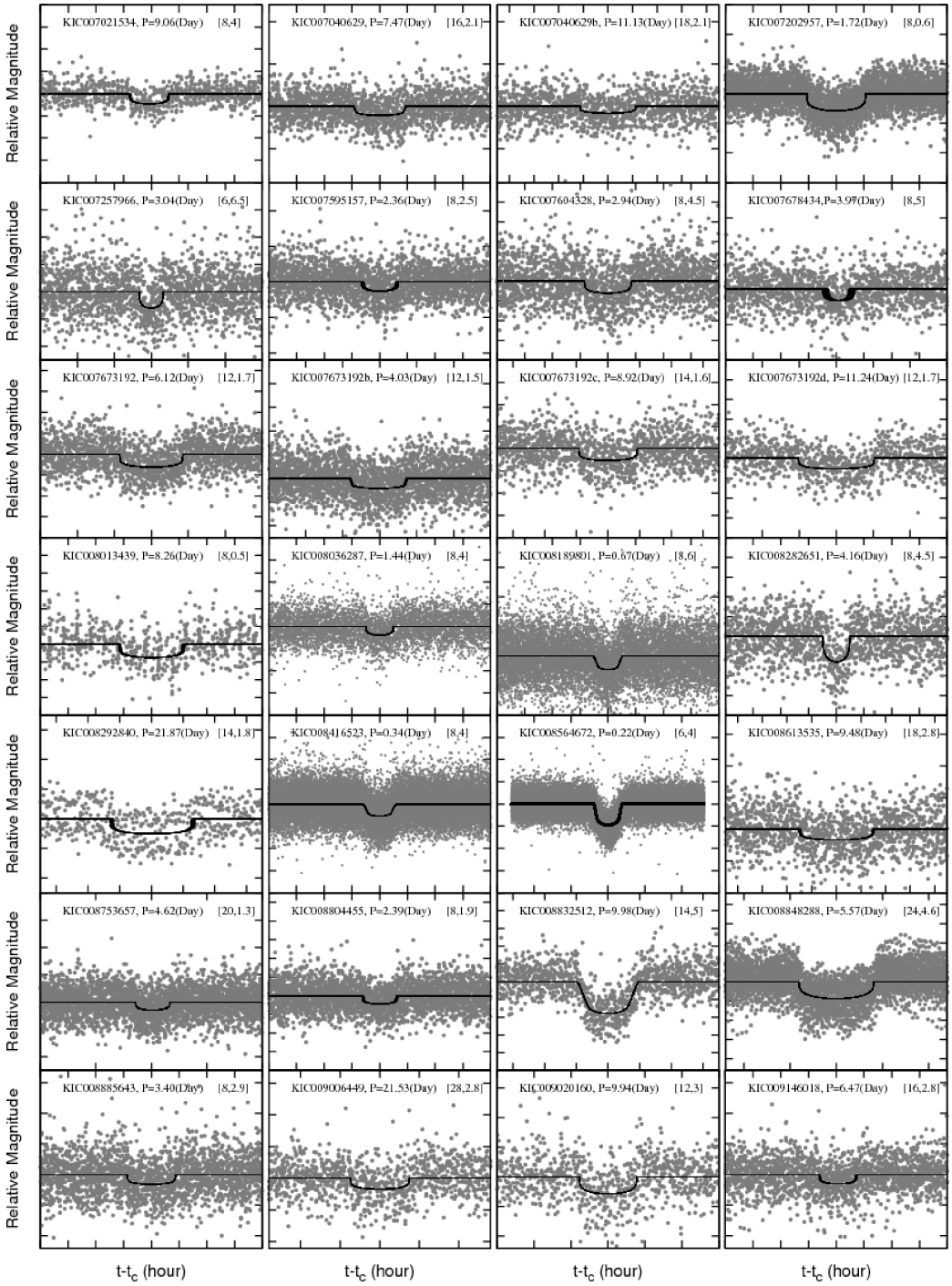

(c)

Figure 8 – *continued*

folded de-trended centroid for both planet candidates in Fig. 13. No anomalous motion is shown in either direction during transit.

KIC 005965819. We found two planet candidates in the system, both with modelled radii less than 2 $R_\oplus$. The inner planet candidate orbits the host star with a period of 8.2 d; the outer planet candidate has a 19.6 d period (see Fig. 8 b, row 3, Columns 1 and 2). They are not in a tight resonance with each other. We note that the transit durations of these two planet candidates are longer than the values expected assuming circular orbits. This might indicate that the planets are in eccentric orbits or the stellar radius of KIC 005965819 is in fact larger than what is listed in the KIC.

KIC 007673192. We found four planet candidates in the system, all with modelled radii around 1 $R_\oplus$. The periods of the candidates are 6.12 d (a), 4.03 d (b), 8.92 d (c) and 11.24 d (d) (see Fig. 8 c, row 3). They are not around any low order resonance pairs. T12 also identified the P=6.12 d signal as a potential transit signal.

KIC 009962455. We found two planet candidates in the system, both with modelled radii around 1 $R_\oplus$. The periods of the candidates

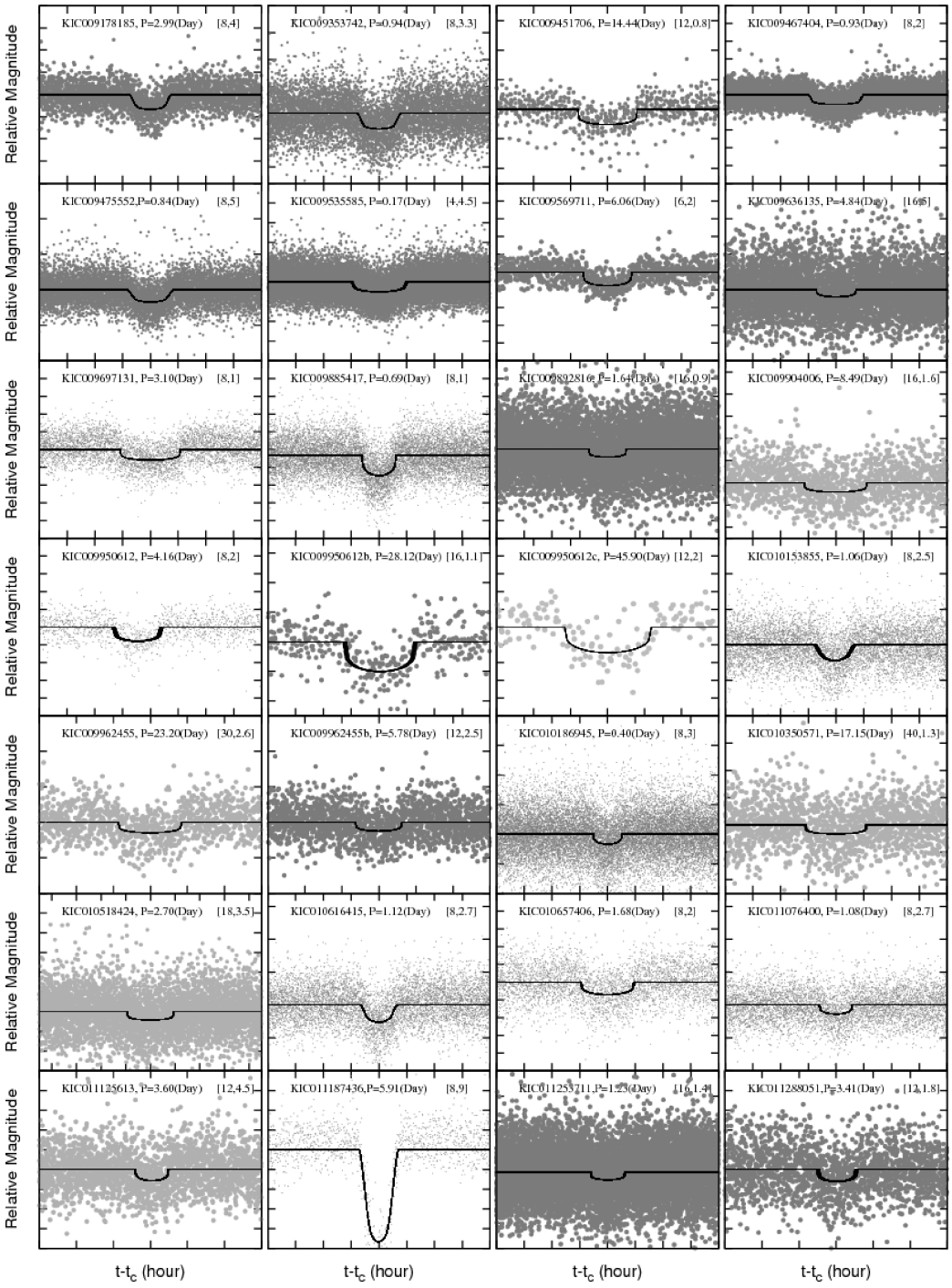

(d)

Figure 8 – *continued*

are 23.20 d (a), 5.78 d (b), in 4:1 resonance (see Fig. 8 d, row 5, Column 2 and 3). The 23.20 d component in the system was also found by T12.

KIC 009535585. The shortest period candidate we found. The signal is modelled as a 1.6 $R_\oplus$ super Earth with a period of only 0.17 d (see Fig. 8 d, row 2, Column 2). If this candidate is confirmed, it would hold the record of the shortest period among the KOIs.

KIC 011253827. We found two planet candidates in the system. The outer planet is Saturn-like with a radius of 6.18 $R_\oplus$ and period of ∼88 d. The inner planet is ∼3.82 $R_\oplus$ with a 43 d period (see Fig. 7, row 6, Column 3 and 4). The Planet Hunters independently found these signals in their web discussion.

KIC 012692087. Also an extremely short-period candidate, really similar to KIC 009535585, with 0.19 d period and 1.5 $R_\oplus$ radii (see Fig. 8 e, row 4, Column 3).

KIC 005689351 (KOI 505). A rich system with potentially as many as three more planet candidates. We initially identified a 2.2 $R_\oplus$ planet candidate with a period of 8.348 d (a) in the system,

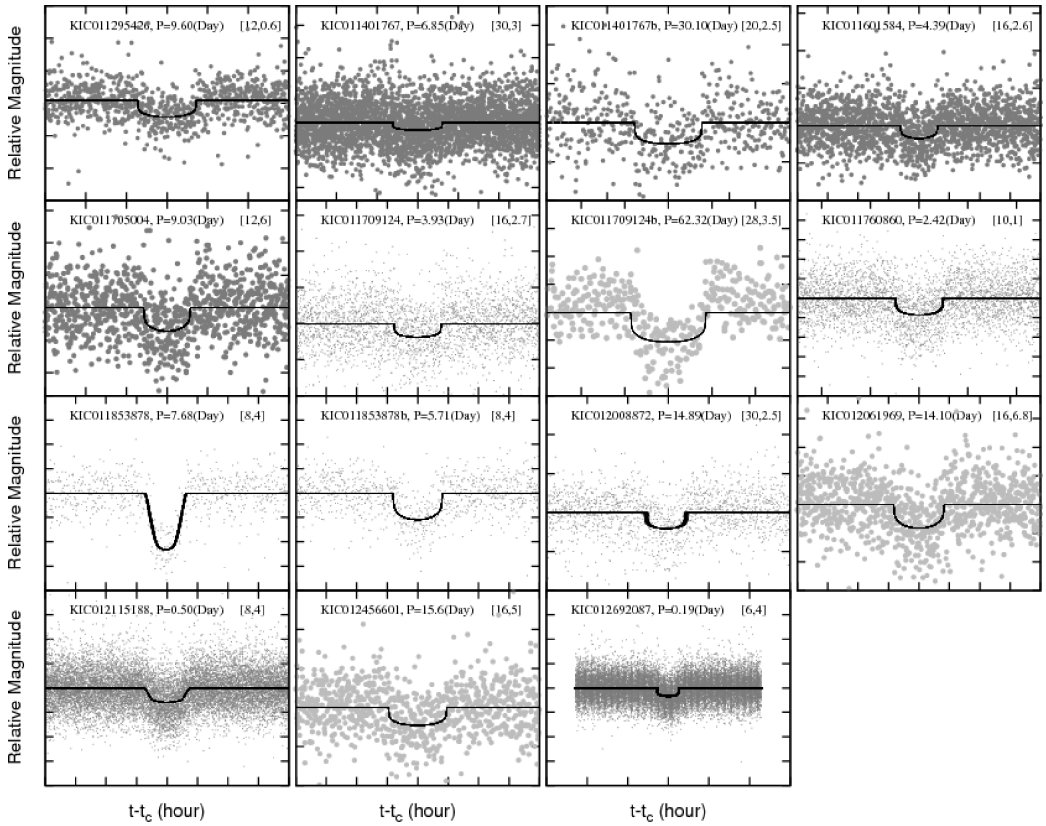

(e)

Figure 8 – *continued*

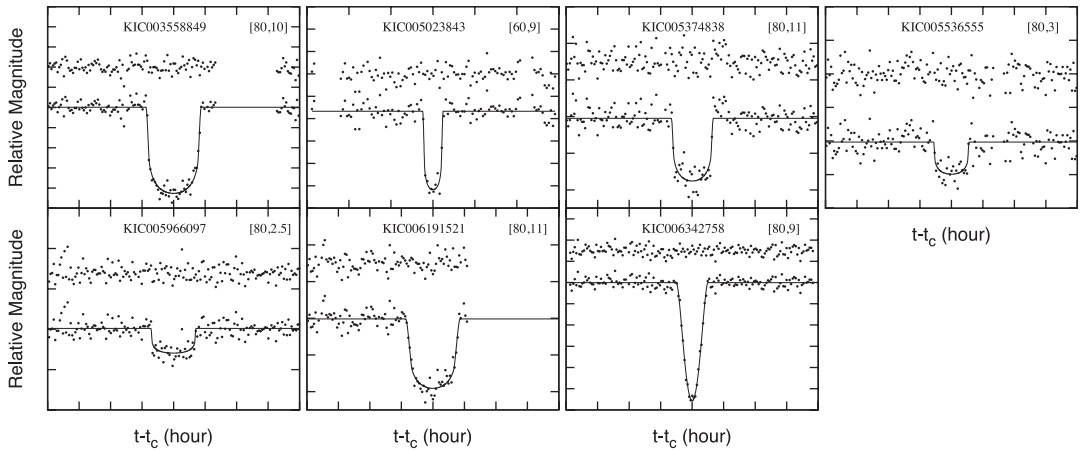

Figure 9. Single transit events. For each candidate we show the best-fitting model on the light curve, together with the residuals from the fit (the configuration is the same as in Fig. 7). The *x*, *y* scales of the subfigure size are marked on the top right, in the units of (h, 1 mmag).

which already has two KOIs. While this paper was under revision, O12 pointed out that there might be two additional signals in the system, with periods of 3.25 d (b) and 87.09 d (c) (see Fig. 8 b, row 3, Columns 1–3). We find the same signals in this light curve after reprocessing the data. The folded light curve of the three planet candidates is separately shown in Fig. 14. When modelling one-planet candidate, we make use of the detected periods and epochs to filter out the transit signals due to the other two. The top and middle panels present the two KOIs, with periods of 13.767 and 6.1956 d. The third planet candidate we found is in a 4:3 resonance with the latter. This is the first reported 3:4:6 resonance three-planet candidate system. Rein et al. (2012) suggest that a resonance chain of three or more planets, in analogue to Jupiter's Moon system, would overcome the difficulties of forming the 4:3 resonance in the traditional way. This system provides an interesting testing-ground for the theory.

KIC 007595157 (KOI 246). A sub-Earth candidate with 0.64 $R_\oplus$ orbiting the star with a period of ∼2.4 d (see Fig. 8 c, row 2, Column 2). It was a single planetary system in B12 catalogue, with KOI 246.01 (1.3 $R_\oplus$ radii and 3.4 d period).

KIC 008753657 (KOI 321). A candidate hot Mars, also the smallest candidate from our new findings, with a modelled radius of

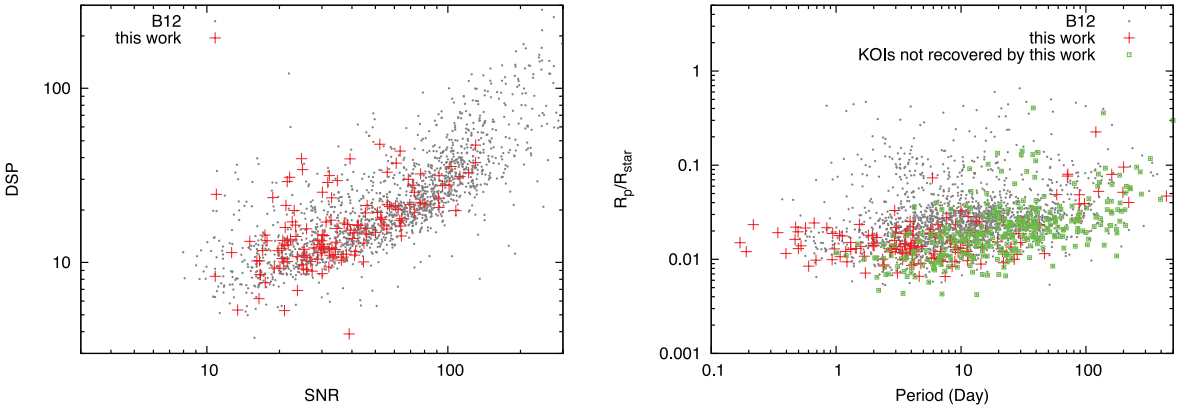

Figure 10. Comparison of KOIs and the planet candidates reported in this paper. Left-hand panel: in SNR-DSP space; right-hand panel: in period-transit depth space. The black dots represent all the KOI planet candidates. The red cross represents the new candidates in this paper. In the right figure, the green squares show the KOIs missed by our searching process.

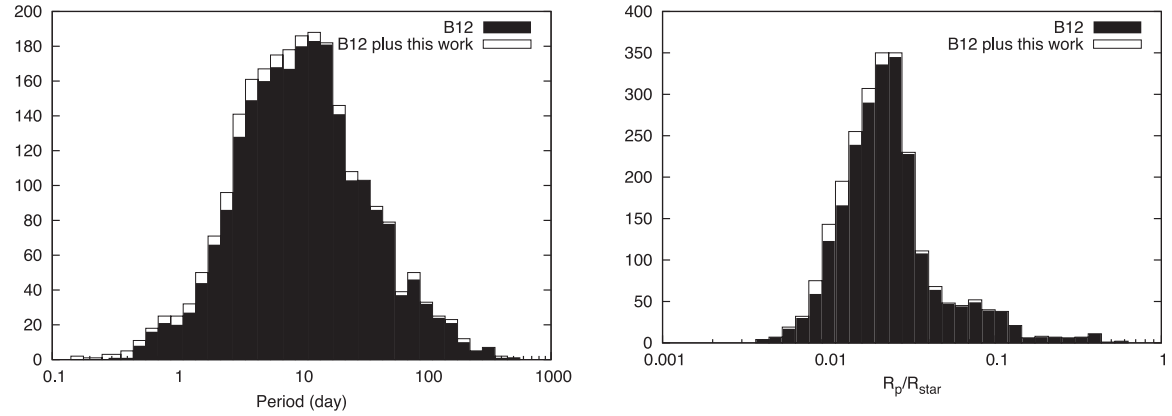

Figure 11. Comparison of the distribution of periods (left) and R_p/R_{star} (right) between KOIs and the total (KOIs and this work). The shadowed regions are the distribution from KOI planet candidates alone.

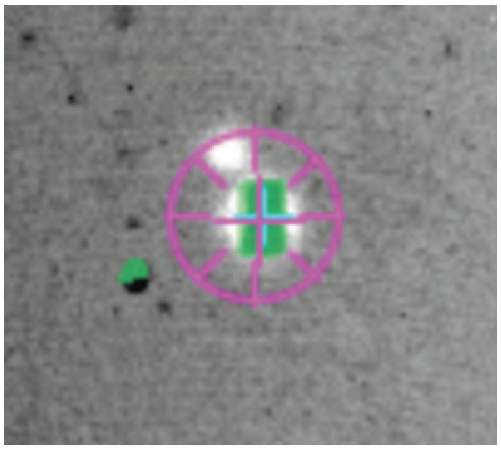

Figure 12. Image of the star KIC 5437945 taken with the APO 3.5-m Echelle slitviewer. The guider is centred on the star. A companion is resolved within ∼5 arcsec.

0.5 $R_\oplus$ and period of 4.6 d (see Fig. 8 c, row 6, Column 1). This is also reported by the Ofir team (O12) with similar modelled parameters. The system was previously known to host KOI 321.01, a 2.4 d candidate superEarth.

KIC 11295426 (KOI 246). B12 catalogue found it to host a superEarth (KOI 246.01) with a 5.38 d period. We found an outer planet candidate with 0.58 $R_\oplus$ radii and 9.6 d period. (see Fig. 8 e, row 1, Column 1). This is also reported by O12.

4 CONCLUSIONS

We have analysed 124 840 stars with public *Kepler* data from quarters Q1–Q6 in total. The large majority of our candidates have already been identified by the *Kepler* team. We recover 92 per cent of Kepler findings from the B11 catalogue and the majority (86.4 per cent of the planet hosting stars and 82.5 per cent of the planet candidates) of the B12 catalogue. 40 new FPs are identified in our analysis of centroids variation. We report 150 new planet candidates and seven *single* transit events that have not been assigned as KOIs in this blind search. 55 of these planet candidates are listed as potential transit signals by the automatic TPS algorithm developed by the *Kepler* team (T12). While this paper was under revision, O12 conducted a search of new planet candidates using the SARS (Simultaneous Additive and Relative System) pipeline in all the KOIs, 43 of the planet candidates in this work overlap with their findings. To our best knowledge, 22 of these planet candidates and three of the single transits are also independently identified by the Planet Hunters in their public website discussion session. 40 of the planet candidates and four of the single transits are reported for the first time.

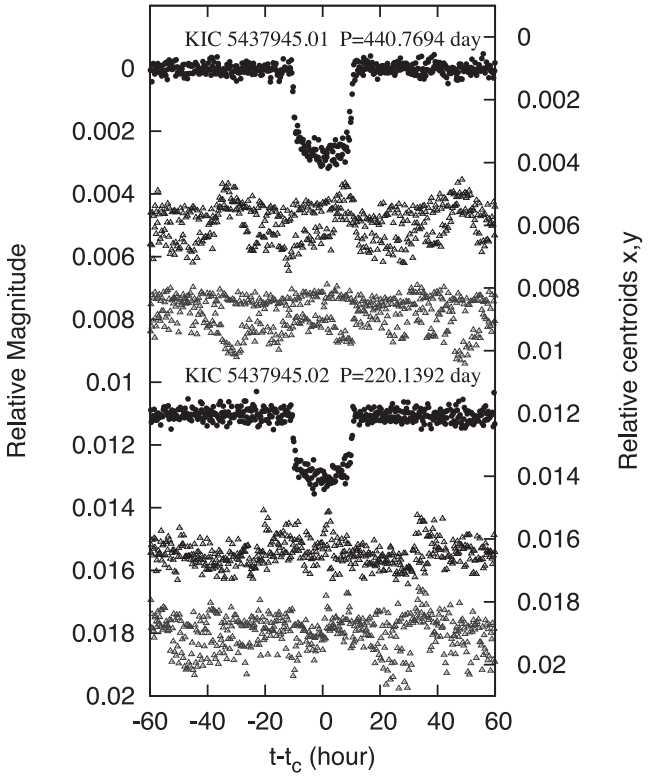

Figure 13. The two planet candidates of star KIC 5437954: from black to grey are the phased folded light curve, and the phased folded x and y direction centroids, all displayed separately. The upper (lower) three plots are for the first (second) planet candidate, with period $P \sim 440(220)$ d. The centroids in the figure are the mean centroids after de-trending.

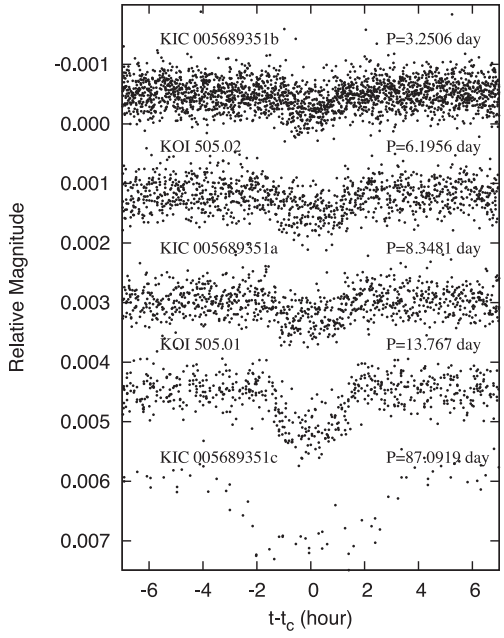

Figure 14. Folded de-trended light curve of KIC 005689351. Each transit is folded relative to its measured epoch, with the signal corresponding to the other planet candidates removed from the light curve. From top to bottom, the periods of the planet candidates are 3.25 d, 6.20 d, 8.35 d, 13.77 d and 87.09 d, respectively. The candidates with periods of 13.77 d and 6.20 d have already been identified as KOI 505.01 and KOI 505.02.

The periods of our new candidates range from $\sim$0.17 to $\gtrsim$ 440 d. The estimated planetary radii vary from $\sim$0.5 $R_\oplus$ to 62 $R_\oplus$. 124 of the planet candidates and three of the single transits have sizes smaller than 3 $R_\oplus$. We also found six new candidate multiple systems. In addition, we found 57 more planet candidates in the already known KOI systems. By comparing our new findings with the Kepler candidates, it appears that for short periods ($<$10 d), our pipeline and search procedure find somewhat more candidates than the Kepler pipeline. Most of the *single* transit events (and a few of the planet candidates) were found by visual inspection of the light curves that were flagged by BLS. This suggests that combining automated searches and visual inspection is an efficient approach for transiting planet searches. Our searching process could potentially act as a supplementation of the findings from the Kepler team to improve the statistics in the short-period planets. We trust that independent searches will benefit both the Kepler team and the community.

ACKNOWLEDGMENTS

We thank the *Kepler* team for the high-quality public data, as well as the PlanetHunter team for their helpful comments. We also thank the anonymous referee for the insightful comments that greatly improved this paper. This research was partly funded by NSF grant AST-1108686.

REFERENCES

Ahmed N. T., Natarajan T. K. R., Rao K. R., 1974, IEEE Trans. Comput., C-23, 90
Bakos G. Á. et al., 2010, ApJ, 710, 1724
Bakos G., Noyes R. W., Kovács G., Stanek K. Z., Sasselov D. D., Domsa I., 2004, PASP, 116, 266
Batalha N. M. et al., 2012, preprint (arXiv:1202.5852) (B12)
Borucki W. J. et al., 2010, Sci, 327, 977
Borucki W. J. et al., 2011a, ApJ, 728, 117
Borucki W. J. et al., 2011b, ApJ, 736, 19 (B11)
Christiansen J. L. et al., 2012a, Kepler Data Characteristics Handbook (KSCI-19040-003)
Christiansen J. L. et al., 2012b, Kepler Data Release 14 Notes (KSCI-19054-001001)
Fischer D. A. et al., 2012, MNRAS, 419, 2900
Ford E. B. et al., 2012, ApJ, 756, 185
Gilliland R. L. et al., 2010, ApJ, 713, L160
Jenkins J. M. et al., 2010a, ApJ, 713, L87
Jenkins J. M. et al., 2010b, ApJ, 713, L120
Jenkins J. M. et al., 2010c, Proc. SPIE, 7740, doi:10.1117/12.856764
Kipping D. M., 2008, MNRAS, 389, 1383
Kipping D., Bakos G., 2011, ApJ, 733, 36
Kipping D. M., Spiegel D. S., 2011, MNRAS, 417, L88
Koch D. G. et al., 2010, ApJ, 713, L79
Kovács G., Zucker S., Mazeh T., 2002, A&A, 391, 369
Kovács G., Bakos G., Noyes R. W., 2005, MNRS, 356, 557
Lintott C. J. et al., 2008, MNRAS, 389, 1179
Lintott C. et al., 2012, preprint (arXiv:1202.6007)
Loeb A., Gaudi B. S., 2003, ApJ, 588, L117
Machalek P. et al., 2010, Kepler Data Release 8 Notes (KSCI-19048-001)
Machalek P. et al., 2011, Kepler Data Release 9 Notes (KSCI-19049-001)
Mandel K., Agol E., 2002, ApJ, 580, L171
Mazeh T., Faigler S., 2010, A&A, 521, L59
Murphy S. J., 2012, MNRAS, 422, 665
Ofir A., Dreizler S., 2012, preprint (arXiv:1206.5347) (O12)
Prša A. et al., 2011, AJ, 141, 83

Rein H., Payne M. J., Veras D., Ford E. B., 2012, MNRAS, 426, 187
Schwamb M. E. et al., 2012, ApJ, 754, 129
Sing D. K., 2010, A&A, 510, A21
Smith J. C. et al., 2012, PASP, 124, 1000
Steffen J. H. et al., 2012, MNRAS, 421, 2342
Tenenbaum P. et al., 2012, ApJS, 199, 24 (T12)
Yee J. C., Gaudi B. S., 2008, ApJ, 688, 616

SUPPORTING INFORMATION

Additional Supporting Information may be found in the online version of this article:

Table 2. Detection report of KOIs.
Table 3. FP list.
Table 4. Stellar parameter table.
Table 5. Planet candidates table. (http://mnras.oxfordjournals.org/lookup/suppl/doi:10.1093/mnras/sts463/-/DC1).

Please note: Oxford University Press are not responsible for the content or functionality of any supporting materials supplied by the authors. Any queries (other than missing material) should be directed to the corresponding author for the article.

This paper has been typeset from a TEX/LATEX file prepared by the author.